

Article

Metabolomic Analysis Reveals the Mechanisms of Hepatotoxicity Induced by Aflatoxin M1 and Ochratoxin A

Ya-Nan Gao^{1,2,3,4,†}, Chen-Qing Wu^{1,2,3,4,†}, Jia-Qi Wang^{1,2,3,4} and Nan Zheng^{1,2,3,4,*}

¹ Key Laboratory of Quality & Safety Control for Milk and Dairy Products of Ministry of Agriculture and Rural Affairs, Institute of Animal Sciences, Chinese Academy of Agricultural Sciences, Beijing 100193, China; gyn758521@126.com (Y.-N.G.); wuchenqing111@163.com (C.-Q.W.); jiaqiawang@vip.163.com (J.-Q.W.)

² Laboratory of Quality and Safety Risk Assessment for Dairy Products of Ministry of Agriculture and Rural Affairs, Institute of Animal Sciences, Chinese Academy of Agricultural Sciences, Beijing 100193, China

³ Milk and Milk Products Inspection Center of Ministry of Agriculture and Rural Affairs, Institute of Animal Sciences, Chinese Academy of Agricultural Sciences, Beijing 100193, China

⁴ State Key Laboratory of Animal Nutrition, Institute of Animal Sciences, Chinese Academy of Agricultural Sciences, Beijing 100193, China

* Correspondence: zhengnan@caas.cn; Tel.: +86-10-62816069

† These authors contributed equally.

Abstract: Aflatoxin M1 (AFM1) is the only toxin with the maximum residue limit in milk, and ochratoxin A (OTA) represents a common toxin in cereals foods. It is common to find the co-occurrence of these two toxins in the environment. However, the interactive effect of these toxins on hepatotoxicity and underlying mechanisms is still unclear. The liver and serum metabolomics in mice exposed to individual AFM1 at 3.5 mg/kg b.w., OTA at 3.5 mg/kg b.w., and their combination for 35 days were conducted based on the UPLC-MS method in the present study. Subsequent metabolome on human hepatocellular liver carcinoma (Hep G2) cells was conducted to narrow down the key metabolites. The phenotypic results on liver weight and serum indicators, such as total bilirubin and glutamyltransferase, showed that the combined toxins had more serious adverse effects than an individual one, indicating that the combined AFM1 and OTA displayed synergistic effects on liver damage. Through the metabolic analysis in liver and serum, we found that (i) a synergistic effect was exerted in the combined toxins, because the number of differentially expressed metabolites on combination treatment was higher than the individual toxins, (ii) OTA played a dominant role in the hepatotoxicity induced by the combination of AFM1, and OTA and (iii) lysophosphatidylcholines (LysoPCs), more especially, LysoPC (16:1), were identified as the metabolites most affected by AFM1 and OTA. These findings provided a new insight for identifying the potential biomarkers for the hepatotoxicity of AFM1 and OTA.

Keywords: aflatoxin M1; ochratoxin A; hepatotoxicity; metabolomics; LysoPCs

Key Contribution: In view of more pronounced metabolic disorders that occurred in the combined treatment group of AFM1 and OTA compared with an individual toxin, we deduced that there was a synergistic effect between AFM1 and OTA in impairing liver tissues. Besides, lysophosphatidylcholines (LysoPCs) were identified as the pivotal compounds after clustering all changed metabolites according to their expression patterns, which was confirmed by the metabolome on human hepatocellular liver carcinoma (Hep G2) cells.



Citation: Gao, Y.-N.; Wu, C.-Q.; Wang, J.-Q.; Zheng, N. Metabolomic Analysis Reveals the Mechanisms of Hepatotoxicity Induced by Aflatoxin M1 and Ochratoxin A. *Toxins* **2022**, *14*, 141. <https://doi.org/10.3390/toxins14020141>

Received: 29 November 2021

Accepted: 21 December 2021

Published: 15 February 2022

Publisher's Note: MDPI stays neutral with regard to jurisdictional claims in published maps and institutional affiliations.



Copyright: © 2022 by the authors. Licensee MDPI, Basel, Switzerland. This article is an open access article distributed under the terms and conditions of the Creative Commons Attribution (CC BY) license (<https://creativecommons.org/licenses/by/4.0/>).

1. Introduction

It has been reported that 25% of agricultural products are contaminated by various mycotoxins [1]. In addition, mycotoxins also occur in some certain indoor spaces such as agricultural product processing places and moldy buildings [2]. Aflatoxin M1 (AFM1) is the only mycotoxin with maximum residue limit (MRL) in milk, 0.50 µg/kg set by China and USA and 0.05 µg/kg set by EU. AFM1 has also been re-identified as Group 1 carcinogen [3].

The high occurrence and contamination levels in milk and milk products were reported in South Asians and Africans as more and more attention has been aroused to monitor AFM1 levels [4]. AFM1 contamination conditions in the Chinese market between 2010 and 2016 were also monitored. Although the quality and safety of milk have improved, AFM1 contamination levels in milk samples occasionally exceeded the legal limit set by the EU [5–7]. Ochratoxin A (OTA) is commonly found in various raw food commodities [8]. In addition, OTA ranked first in the prevalence of cereals foods based on 9627 samples by meta-analysis [9]. IARC classified OTA as Group 2B carcinogen [10,11]. The co-occurrence of these two toxins has been reported in milk and baby food samples [12–14]. On the other hand, AFM1 and OTA also may co-exist in certain organic dust originating from cereal [15]. Given that the co-existed mycotoxins may perform different interactive effects including additive, synergistic, or antagonistic effects, consequently, the potential risk of exposure to both AFM1 and OTA could not be underestimated.

Given that the major target organ of aflatoxins (AFs) is the liver, several studies have demonstrated its liver toxicity. A meta-analysis showed that the increased risk of liver cirrhosis is associated with AFs exposure [16]. AFB1 significantly resulted in acute liver injury in rats, including hepatic histopathological damage and abnormal liver function [17]. It has been demonstrated that AFB1-induced hepatotoxicity via oxidative stress and apoptosis or autophagy [18,19]. Although OTA targets the kidney, it also involves liver injury. OTA could result in liver oxidative stress and inflammation in animal models, including mice, duck, and weanling pigs [20–23].

In this study, we tried to find out the potential mechanisms of hepatotoxicity induced by AFM1 and OTA. It has also been reported that metabolomics could demonstrate the metabolic changes and identify the biomarkers [24]. Therefore, metabolomics was conducted in the model of CD-1 mice and HepG2 cells. These findings will provide new insights into combined toxic effects of different mycotoxins in daily foods and the environment.

2. Results

2.1. AFM1 and OTA-Induced Liver Injury in Mice

The bodyweight of mice was recorded over 35 days (Figure 1A). Compared with the control group, there was no significant difference in the DMSO vehicle group of final weight ($p > 0.05$), while individual AFM1 and OTA as well as their combination significantly decreased the weight ($p < 0.05$, Figure 1B). The liver weight was significantly decreased in the combination of AFM1 and OTA group ($p < 0.05$, Figure 1C), while no significant difference was shown in the liver index ($p > 0.05$, Figure 1D). The serum indicators related to liver injury (ALT, AST, TBIL, and GCT) were evaluated (Figure 1E–H). Compared with the control group, the level of these four serum biochemical parameters was significantly increased in the combination of the AFM1 and OTA groups ($p < 0.05$). Haematoxylin-eosin (HE) and oil red O (ORO) staining was used to investigate the effects on liver morphology and the extent of lipidation (Figure 2). The staining results of HE showed that toxins, especially for the combined treatment, caused liver damage, including poor cytoplasm, inflammatory infiltration, dilation of sinusoids, and irregular shape of the nucleus (marked by yellow arrows) (Figure 2A). The ORO staining results showed that liver steatosis occurred in the toxin treatment group and the percentage of lipid droplet area in the toxins combination group was significantly increased compared with the control group ($p < 0.05$, Figure 2B,C).

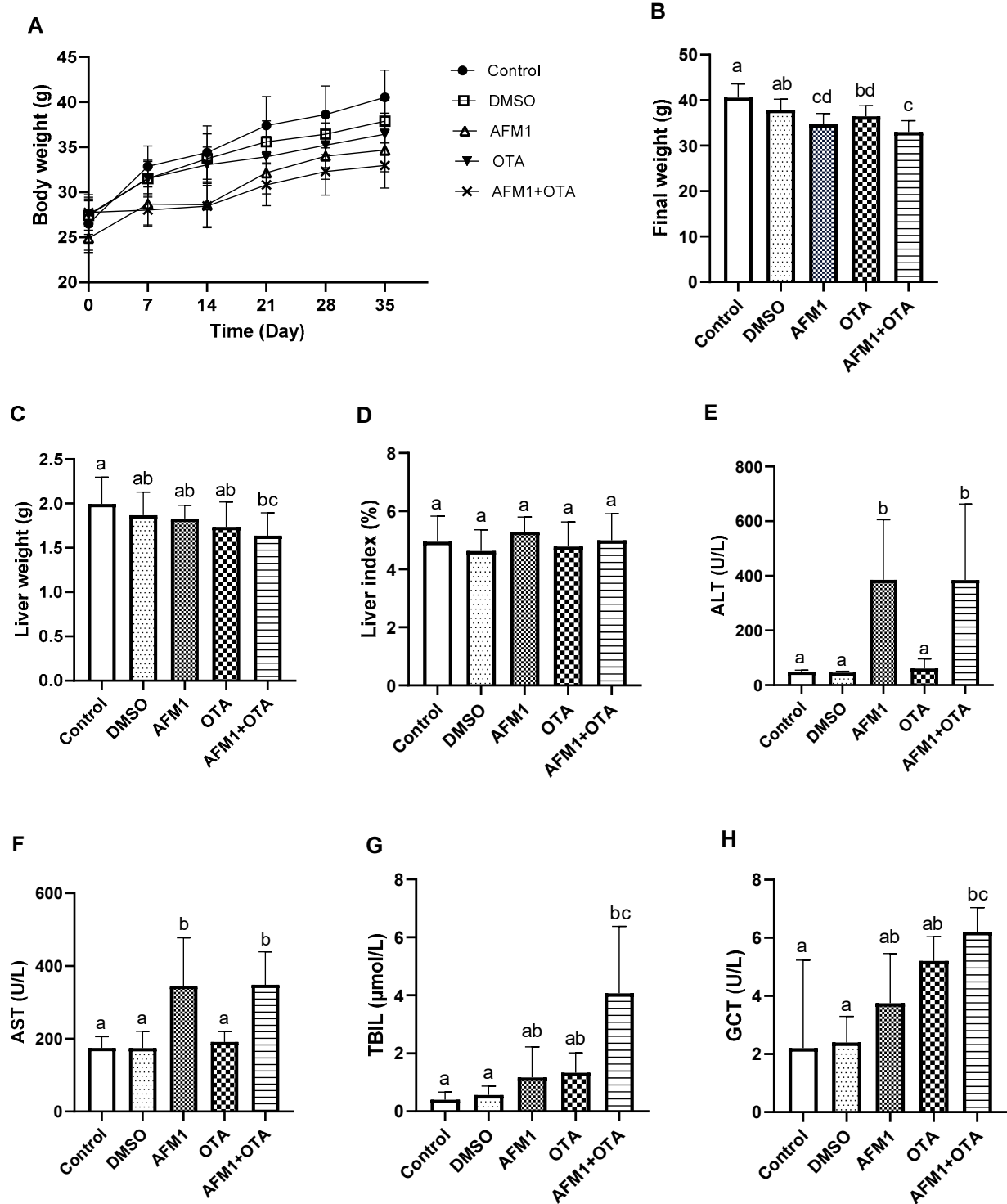


Figure 1. Effects of individual and combined AFM1 and OTA on body weight, liver index, and serum biochemical indicators of mice. (A) body weight-time growth curve, (B) final body weight, (C) liver weight, (D) liver index, (E) alanine aminotransferase (ALT), (F) aspartate aminotransferase (AST), (G) total bilirubin (TBIL), and (H) glutamyltransferase (GCT). Results are represented as mean \pm SD ($n = 12$). Different letters (a,b,c,d) indicate significant differences ($p < 0.05$). Control represents the untreated group, DMSO represents the DMSO vehicle group, AFM1 represents AFM1 at 3.5 mg/kg b.w., OTA represents OTA at 3.5 mg/kg b.w., and AFM1+OTA represents the combined AFM1 and OTA group (3.5 mg/kg b.w. + 3.5 mg/kg b.w.).

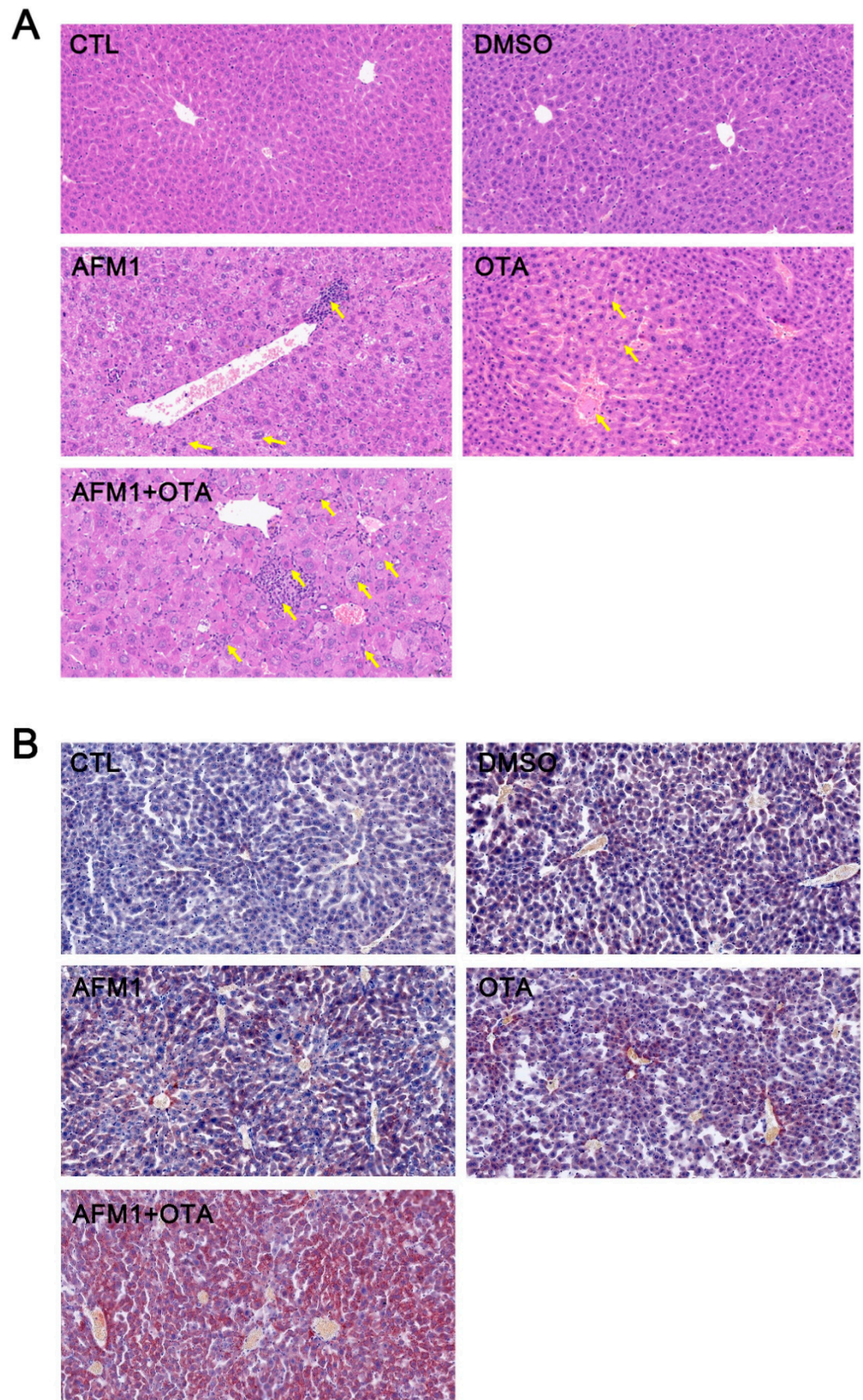


Figure 2. Cont.

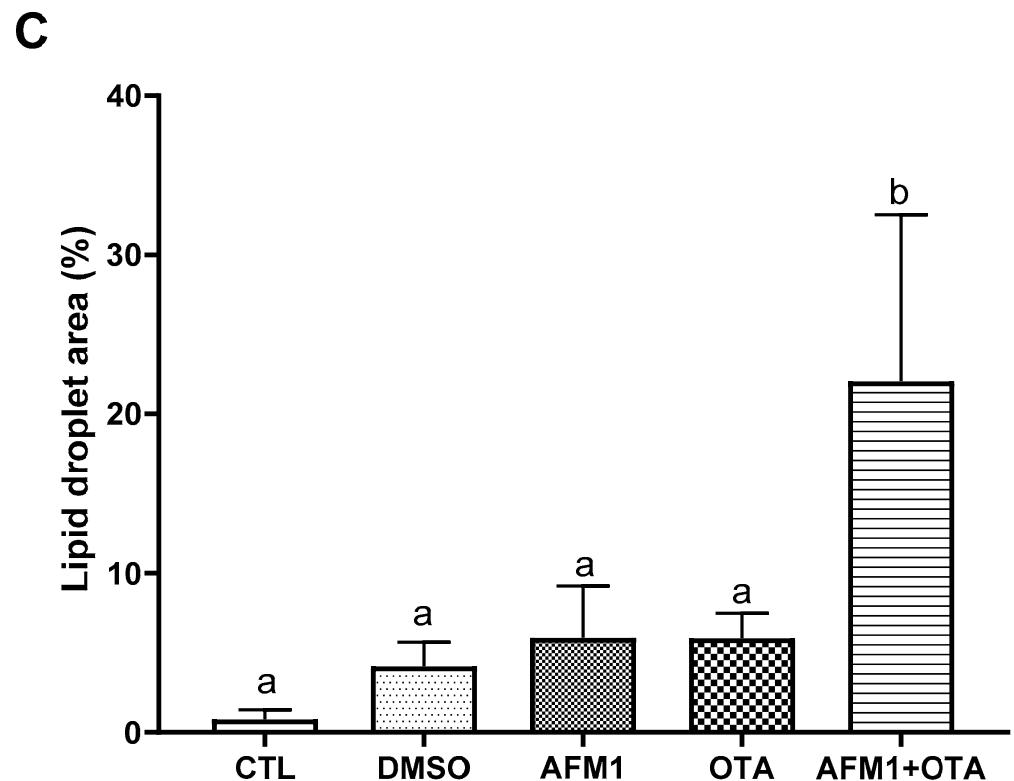


Figure 2. Histopathological examination of control, DMSO, AFM1, OTA, and AFM1+OTA-treated liver tissues by (A) hematoxylin and eosin (HE) (400×) staining, (B) oil red O (200×) and (C) the percentage of lipid droplet area. Different letters (a,b) indicate significant differences ($p < 0.05$). CTL represents the untreated group, DMSO represents the DMSO vehicle group, AFM1 represents AFM1 at 3.5 mg/kg b.w., OTA represents OTA at 3.5 mg/kg b.w., and AFM1+OTA represents the combined AFM1 and OTA group (3.5 mg/kg b.w. + 3.5 mg/kg b.w.).

2.2. Multivariate Analysis of the Metabolic Profiles

Metabolomics data of liver and serum was examined through two-dimensional unsupervised PCA to observe the variance and distribution of samples within and between different treatments. The PCA analysis showed that no samples were separated in each group, so all samples were reserved in the subsequent analysis (Figure 3A,C). The supervised OPLS-DA analysis was performed to characterize the metabolite profile in the liver and serum. As illustrated in Figure 3B, DMSO treatment cannot be completely separated from the control group for the liver metabolites, while both individual and combined toxin treated groups were clearly separated from the control group. Similar results were also shown in the serum metabolites (Figure 3D). In addition, both in liver and serum, compared with the AFM1 treatment, OTA treatment was closer to the combined toxins treatment, indicating that OTA exerted a stronger hepatotoxicity in mice.

2.3. Identification of Differential Metabolites of Mice

In total, 142 and 169 metabolites were identified by UPLC-MS analysis in mice liver and serum, respectively. The integral metabolic network that contained all identified metabolites in liver and serum among DMSO vehicle, individual, and combined toxins group were depicted in Figures 4 and 5. For the liver, compared with the DMSO vehicle group, the highest number of changed metabolites was present in the AFM1 + OTA group (10 up-regulated and 37 down-regulated), followed by the AFM1 group (13 up-regulated and 9 down-regulated) and OTA group (9 up-regulated and 11 down-regulated) (Figure 4). For serum, the highest number of changed metabolites was also shown in the AFM1 + OTA treatment (20 up-regulated and 28 down-regulated), followed by OTA treatment (29 up-

regulated and 14 down-regulated) and AFM1 treatment (5 up-regulated and 27 down-regulated) (Figure 5). The results compared with the control group (Figures S1 and S2) were similar to the results compared with the DMSO group. These results suggested that the combined AFM1 and OTA displayed the synergistic effect and OTA might be the one that exerted chief toxic effect.

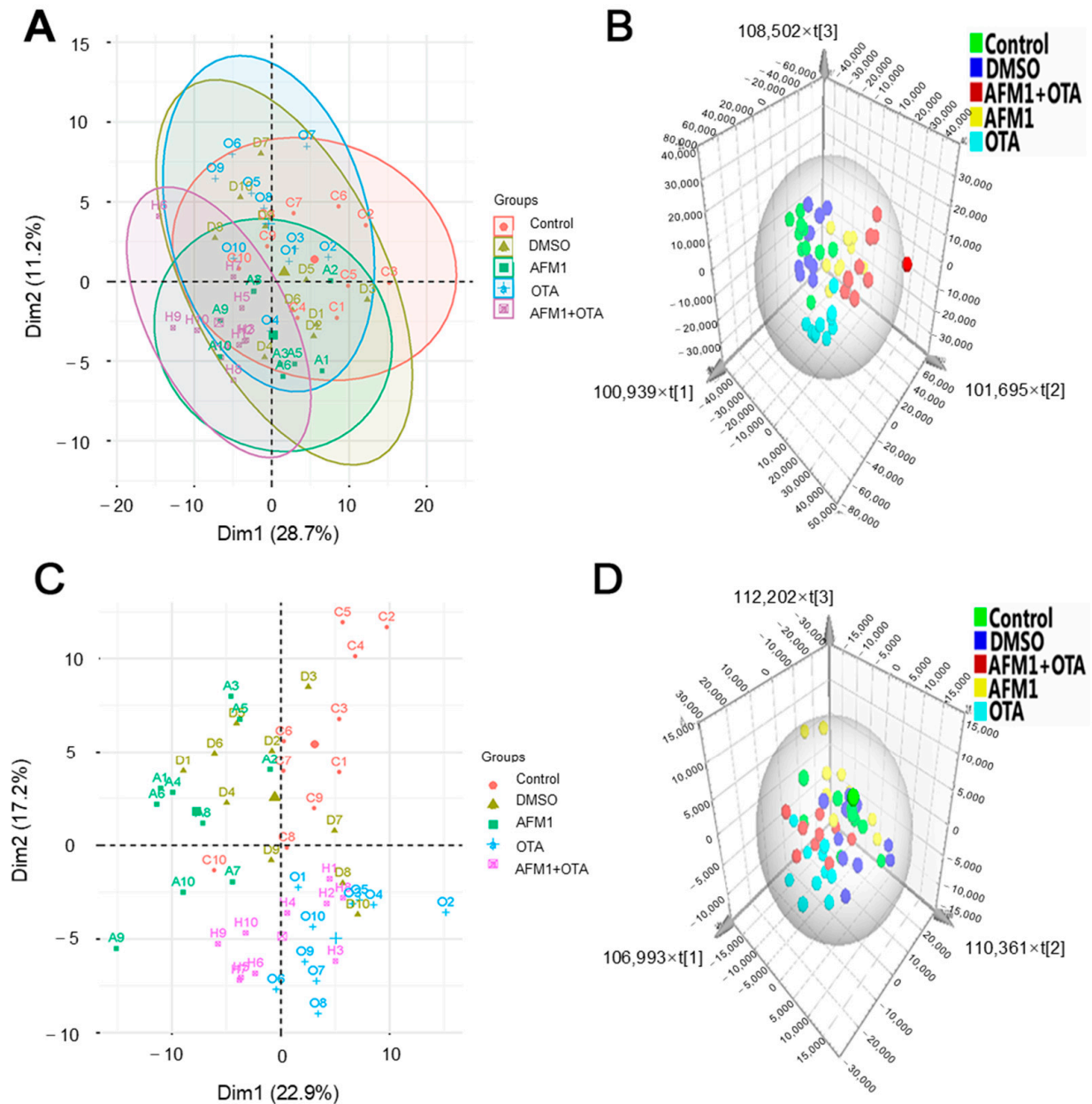


Figure 3. PCA score plots and OPLS-DA analysis of liver and serum samples. (A) The scores plot of PCA in the liver, (B) the scores plot of PLS-DA in the liver, (C) the scores plot of PCA in serum, (D) the scores plot of PLS-DA in serum. C represents the untreated group (Control), D represents the DMSO vehicle group (DMSO), A represents AFM1 at 3.5 mg/kg b.w. (AFM1), O represents OTA at 3.5 mg/kg b.w. (OTA), and H represents the combined AFM1 and OTA group (3.5 mg/kg b.w. + 3.5 mg/kg b.w.) (AFM1+OTA).

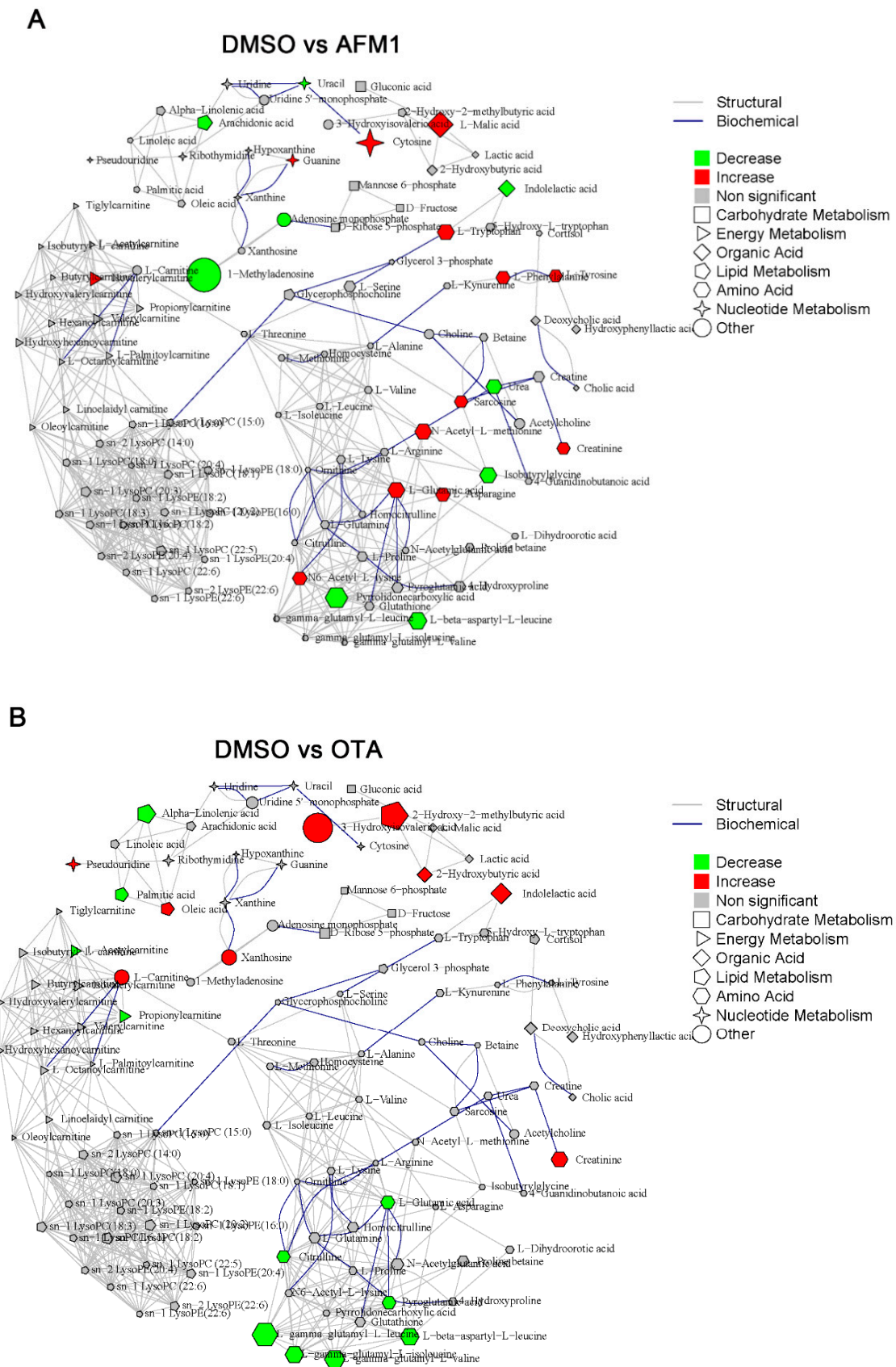


Figure 4. Cont.

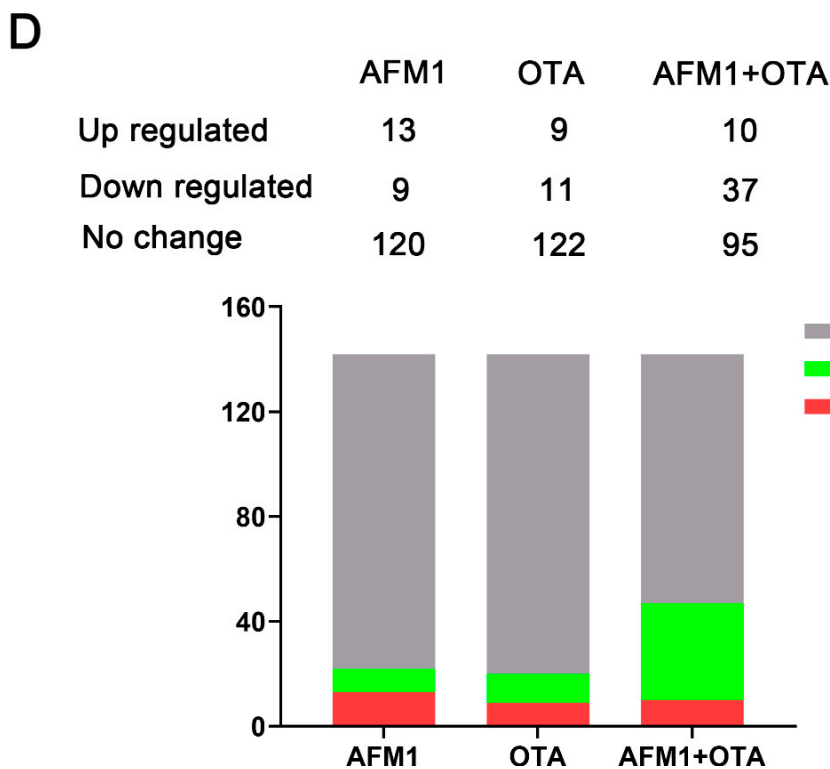
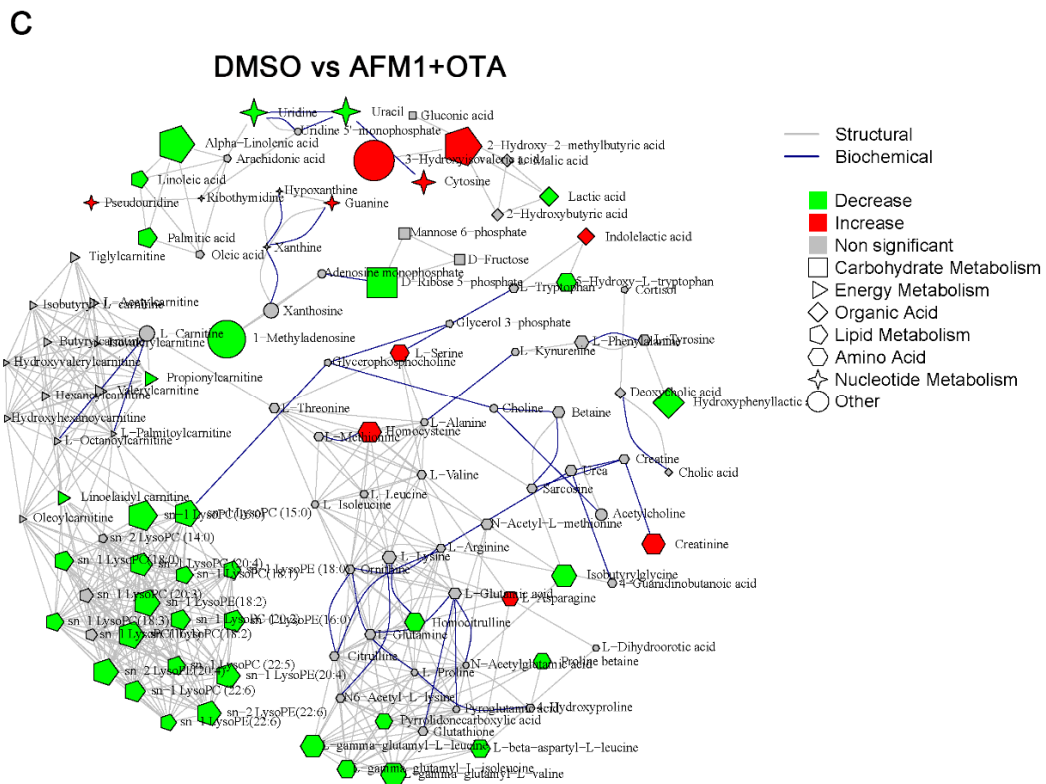
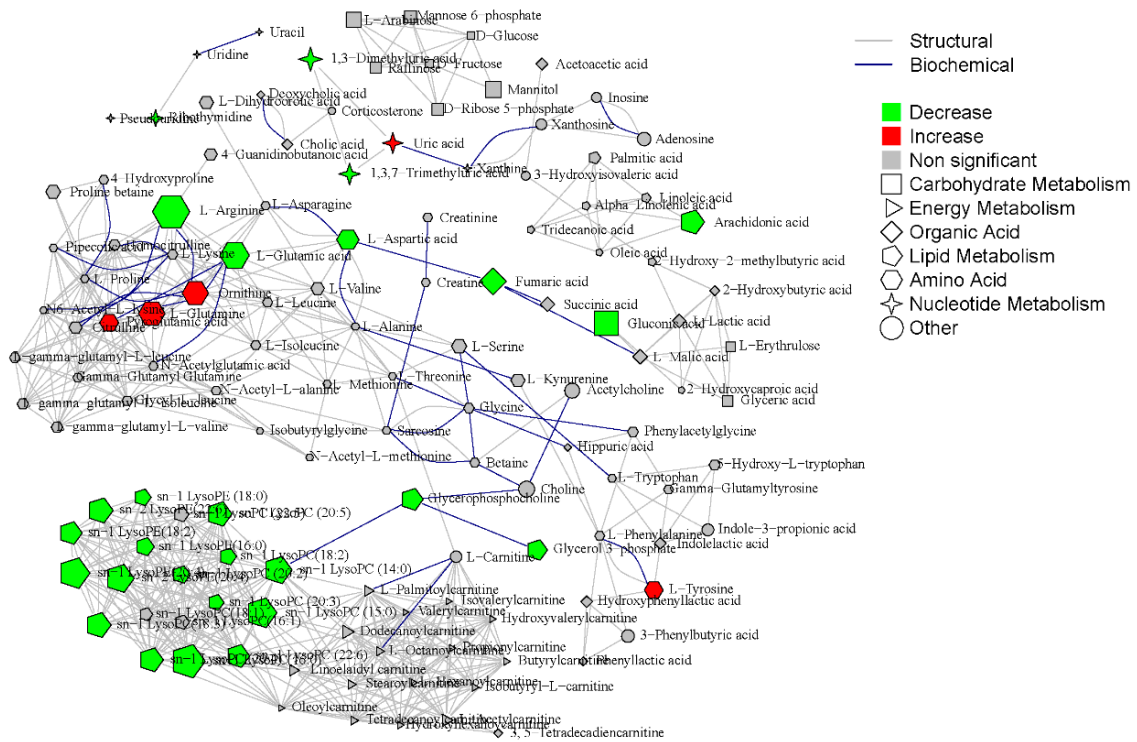


Figure 4. Metabolite integrated metabolic pathway analysis in liver of mice treated with individual and combined AFM1 and OTA. (A) DMSO vs. AFM1, (B) DMSO vs. OTA, (C) DMSO vs. AFM1+OTA, and (D) the number of changed metabolites in different mycotoxins treatment. Red represents the upregulated metabolites and the green represents the downregulated metabolites with criterion of FC > 1.50, and $p < 0.05$.

A

DMSO vs AFM1



B

DMSO vs OTA

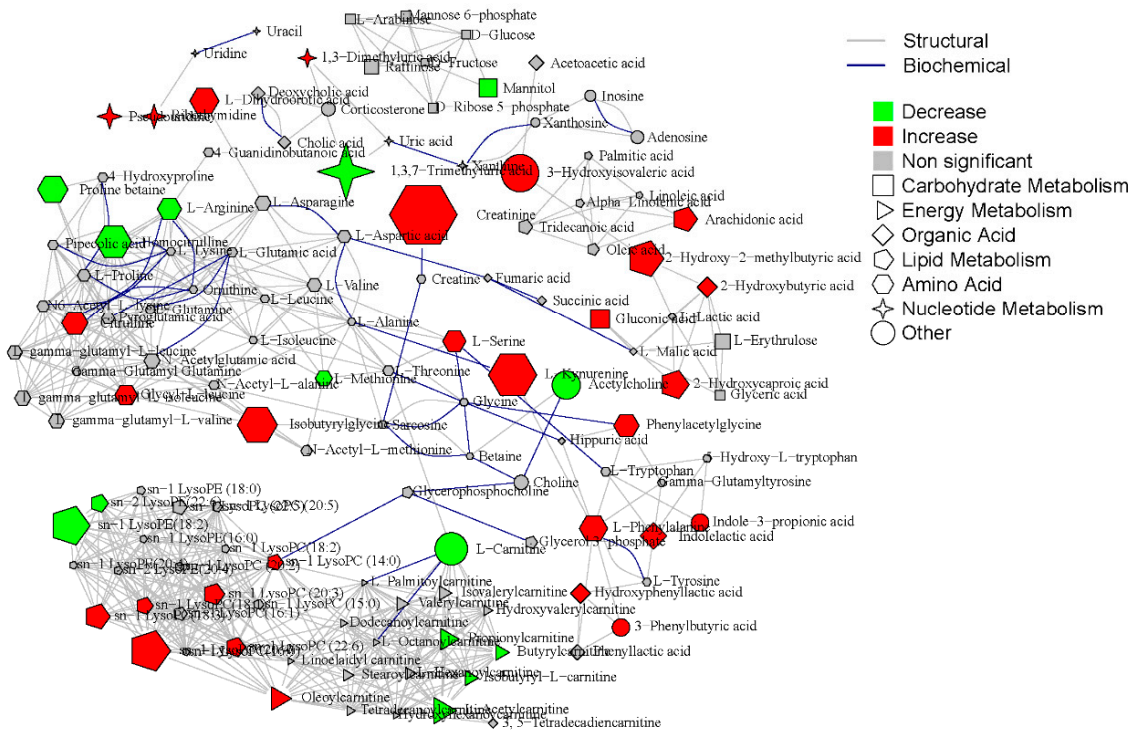


Figure 5. Cont.

2.4. The Main Type of Metabolites Affected by AFM1 and OTA

The heatmap analysis was used to visually compare the metabolome levels among samples and treatments (Figure 6). The metabolites in the heatmap were clustered based on their expression levels, and these results depicted that the metabolic patterns among control treatment, DMSO vehicle treatment, and AFM1 treatment were similar, which were significantly different from OTA and AFM1+OTA treatment. These results were consistent with Figure 4, Figure 5 and Figure suggesting that OTA might serve as the predominant toxicity in the combination of AFM1 and OTA. In addition, as the results depicted in Figure 6, among the 20 significant altered metabolites both in liver and serum, LysoPCs were the main type metabolites affected by AFM1 and OTA. Moreover, the concentration of changed LysoPCs in the liver and serum was shown in Figures S3 and S4. Furthermore, to more accurately target the differentially expressed metabolites, we conducted the metabolism of HepG2 cells. The concentration of AFM1 (1 µg/mL) and OTA (0.05 µg/mL) was used for metabolome analysis based on cell viability (Figure S5). The metabolites heatmap of HepG2 cells also demonstrated that LysoPCs were involved in the liver toxicity induced by AFM1 and OTA (Figure S6). The expression pattern of LysoPCs in HepG2 cells was similar as in serum (Figure S7). More specially, we found that sn-1 LysoPC (16:1) was the most crucial LysoPCs in the hepatotoxicity induced by the combination of AFM1 and OTA, and its concentration in mice and Hep G2 cells is shown in Figure 7.

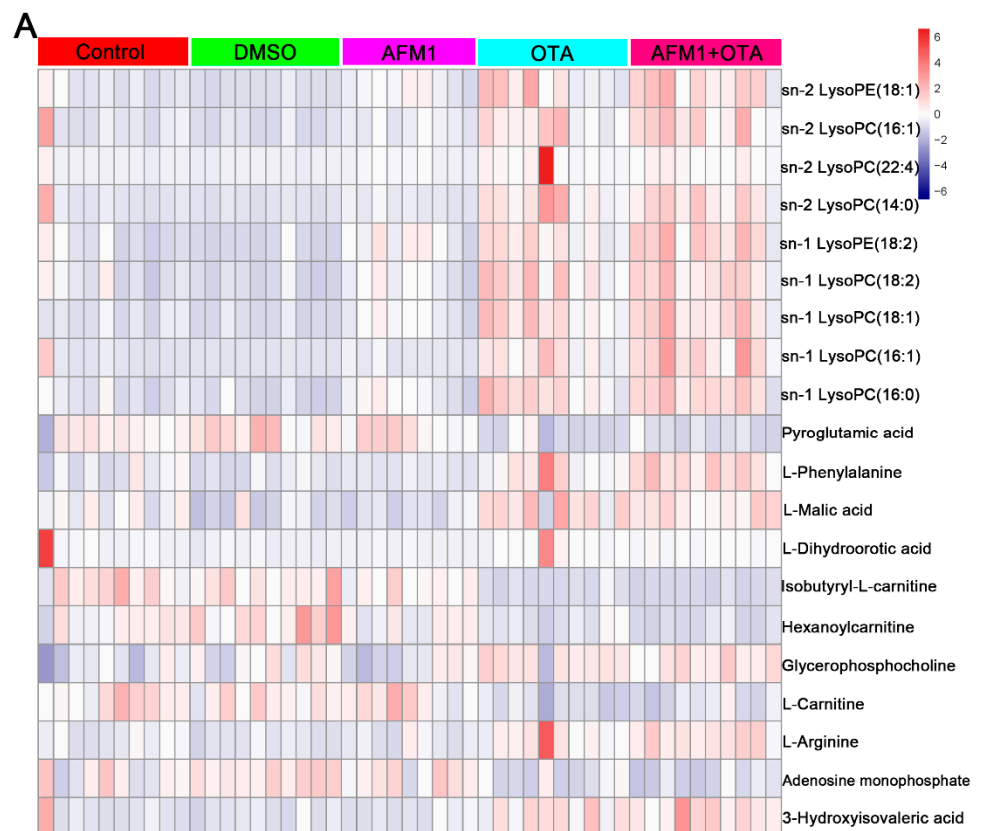


Figure 6. Cont.

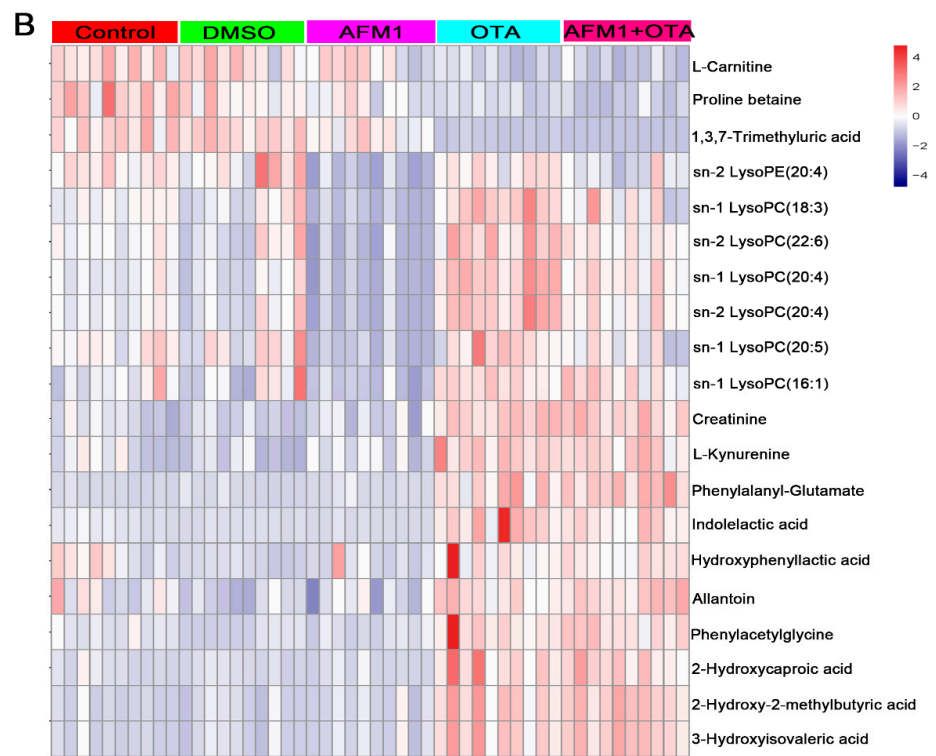


Figure 6. Heat map representation of metabolites mice under different conditions of mycotoxins treatment. (A) liver tissue and (B) serum samples. Red and blue represent higher and lower level of the respective metabolites.

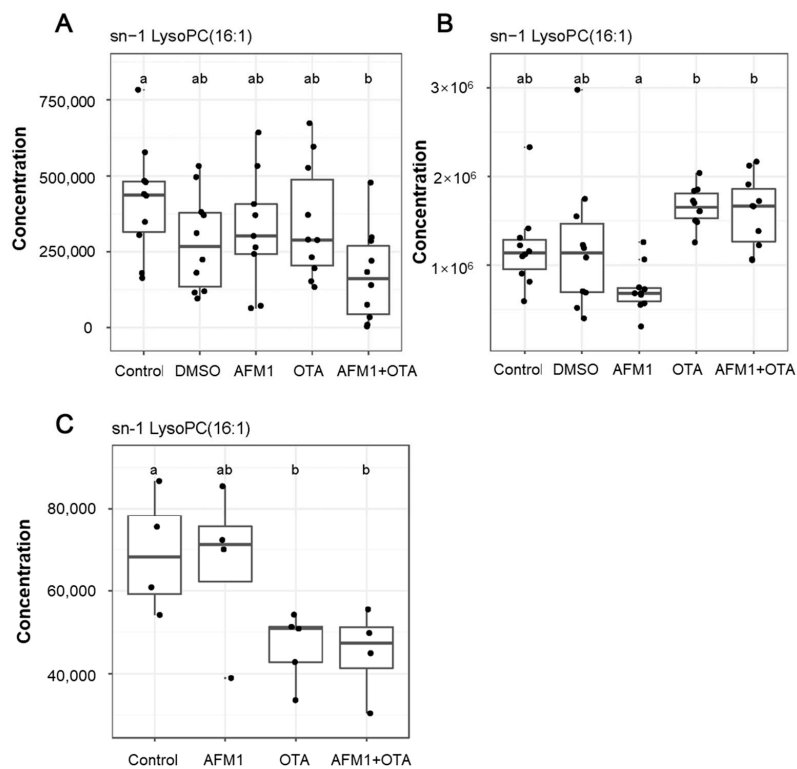


Figure 7. Boxplots of AFM1, OTA and AFM1+OTA regulation of co-differential metabolites in mice (A) liver and (B) serum as well as (C) HepG2 cell.

3. Discussion

It is common to find the co-contamination of AFM1 and OTA in the environment. The liver not only plays a vital role in metabolism but also plays a key role in detoxification and excretion of exogenous chemicals [25]. Therefore, it is reasonable to determine the adverse effects caused by AFM1 and OTA on liver tissue and expound on the potential mechanism(s). Given that various interaction types exert in the combined mycotoxins, the interactive effects between AFM1 and OTA also needed to be clarified. In the present study, *in vivo* (CD-1 mice) and *in vitro* (HepG2 cells) models were used and analyzed by metabolomics. Our results showed that AFM1 and OTA led to liver tissue damage, which was associated with LysoPCs metabolites. Moreover, their combination performed a synergistic interactive effect, in which OTA exerted the dominant hepatotoxicity role.

The serum biochemical parameters (ALT, AST, TBIL, and GCT) are considered to be indicators for liver impairment. In the present study, AFM1 and its combination with OTA significantly affected the level of these indicators (Figure 1). In normal conditions, ALT and AST mainly present in the liver tissue. When the liver is damaged, part of the ALT and AST in the liver tissue will enter the blood, which will eventually lead to the increase in the activity of ALT and AST in the serum [26]. Broilers exposed to dietary AFB1 caused significantly increased activity of ALT and AST in serum [8]. It has been reported that injured liver and bile duct could lead to increased serum TBIL levels [27]. The increased TBIL concentration was found in the mice fed with 1.5 mg/kg AFB1 for seven days [28]. The level of GCT, a cholestatic liver enzyme, will increase during liver dysfunction [29]. The activity of liver cytosolic GST in broilers exposed to AFB1 was increased for 7, 21, and 42 days [30].

The phenotypic results *in vivo* demonstrated that the combined AFM1 and OTA produced more serious adverse effects on liver damage than individually groups (Figures 1 and 2), which indicated that their combination displayed a synergistic effect. Various interactive effects were exerted in combined mycotoxins. The studies regarding the interaction of combined mycotoxins mainly focused on the models *in vitro* [31–33]. Only two studies reported the interactive effects of mycotoxins *in vivo*. The interactive effect between AFB1 and deoxynivalenol (DON) was synergism on the injured liver-related parameters including ALT, AST, and albumin (ALB), while the combination of AFB1 and zearalenone (ZEA) produced an antagonistic effect in those parameters [34]. It had been reported that the combination of DON and ZEA displayed an antagonistic effect in the liver tissue of mice [35]. The combined *in vivo* and *in vitro* studies regarding the hepatotoxicity of mycotoxins were limited. Only one research demonstrated that synergistic hepatotoxicity was proved in the combined patulin and cadmium *in vivo* (C57BL/6N mice) and *in vitro* (AML12 cells) [36]. Therefore, the *in vivo* results of combined toxins filled the gap to a certain extent.

In the present study, we applied the mice liver and serum metabolomics *in vivo* combined with *in vitro* (HepG2 cells) to explore the underlying mechanisms for the hepatotoxicity induced by AFM1 and OTA. The metabolomics of individual liver or serum has been used to characterize toxicological outcomes induced by various hazard factors, such as ethanol and silica nanoparticles [37–39]. However, the combined metabolomics of liver and serum is relatively insufficient. Hepatic and serum metabolomics were applied in the toxicity study of individual chemicals of psoralen and bisphenol A [40,41]. More importantly, there were only two studies using metabolomics to expound the interactive effects of combined mycotoxins [35,42]. Therefore, the findings in this study with the combined liver and serum metabolomics on the hepatotoxicity interactive effects of AFM1 and OTA could broaden our horizons. The number of differentially expressed metabolites in combined toxins was higher than individual mycotoxins (Figures 4D and 5D), suggesting that the synergistic effect was exerted, which was consistent with the phenotypic results.

In the present study, the metabolomics analysis *in vivo* and *in vitro* provides a possibility to screen the key functional metabolites more accurately, and we found that lysophosphatidylcholines (LysoPCs), more specially sn-1 LysoPC (16:1), played a vital role in the hepatotoxicity induced by AFM1 and OTA. There were some discrepancies in the expression

pattern of LysoPCs in tissue and HepG2 cells, which could be partially explained by the differences between cells and the whole animal body. Metabolomics analysis demonstrated that the potential biomarkers for hepatocellular carcinoma (HCC) disease were taurocholic acid, lysophosphoethanolamine (LysoPE) 16:0, and LysoPC (22:5) [43]. The analysis of human plasma metabolic profiling suggested that LysoPCs, especially LysoPC (18:1), LysoPC (18:2), LysoPC (20:3), LysoPC (20:4), LysoPC (22:6) were the significantly altered metabolites that have the preventive effect against liver diseases and anti-inflammatory effects [44]. Rats exposed to chronic low-dose acrylamide led to the significant changes of LysoPE (18:3), LysoPE (20:5), and LysoPC (20:4) in the liver [45]. Clinical serum metabolomics demonstrated that the development of liver cirrhosis was related to the levels of metabolites including LysoPC (22:6), myristic acid, and palmitic acid [46].

Phosphatidylcholines (PC) and phosphatidylethanolamines (PE) have been demonstrated to be associated with steatosis and phospholipidosis [47]. PCs and LysoPCs are negatively correlated, depending on the membrane function synthesis of PCs, and the catalysis of PCs, which could induce lipo-apoptosis [48]. It has been observed that the correlation between acylcarnitine and LysoPC is negatively correlated with PC, assuming that LysoPC is recruited from PC or inhibits PC formation [49]. In this study, serum metabolic profiling showed that the increased level of LysoPCs and decreased level of L-carnitine were performed in toxins treatment. Moreover, the up-regulated LysoPCs could result in cell apoptosis via triggering reactive oxygen species (ROS) production [50,51]. In addition, it has been reported that ROS progress could activate extracellular hydrolyzed by phospholipase A2 (PLA2), and hydrolyze PCs to accumulate LysoPCs [52]. However, during oxidative stress, when LysoPCs combine with acyl groups to form PCs, the down-regulation of LysoPCs may also be related to the toxicity mode [53], which could explain why the concentration of LysoPCs in the liver decreased. L-carnitine has been previously proven to prevent the formation of ROS [54,55]. Accordingly, we speculated that AFM1 and OTA may lead to the oxidative stress of mice liver, inducing the changes in metabolites, eventually damaging the liver. The possible mechanisms of different effects on oxidative damage caused by individual AFM1 and OTA were reported in a previous study [56]. The lipophilic structure of these two toxins and their competition for glutathione in cells could partly explain, the deviations of cytotoxicity induced by AFM1 and OTA, and further studies are needed to research the exact mechanisms.

Except for hepatotoxicity, the toxicology induced by AFM1 and OTA also had been reported by previous studies. Metabolomics analysis showed that when AFM1 and OTA were combined together, OTA exhibited the dominant effect on the alteration of kidney metabolic processes [57], which was consistent with the role of OTA in the present study. The synergistic effect of the combined AFM1 and OTA was demonstrated in disrupting intestinal integrity, including the decreased cell viability and the expression of tight junction proteins as well as mucins, as well as the increased epithelial permeability and intestinal inflammation [56,58–61]. The synergy was also consistent with the combined effect on hepatotoxicity induced by AFM1 and OTA in the present study.

In summary, we assess the hepatotoxicity of AFM1 and OTA in the CD-1 mice model. The phenotypic results and metabolomics analysis *in vivo* demonstrated that the combination of AFM1 and OTA performed more serious adverse effects on mice liver, displaying the synergistic effect, in which OTA performed the dominant role. This finding suggested that although the carcinogen classification level of AFM1 (Group 1) is higher than that of OTA (Group 2B), the adverse effects of OTA cannot be ignored. And this finding also provided a basis that OTA should be classified as a higher level of human carcinogen as previous studies demonstrated [10,11]. In addition, the limit standard for OTA in milk should also be considered to establish due to its higher hepatotoxicity than AFM1. By means of the combined metabolomics analysis *in vitro* and *in vivo*, we found that LysoPCs, especially, LysoPC (16:1) were the main type of metabolites affected by AFM1 and OTA, which are related to oxidative stress, resulting in the hepatotoxicity. In order to more accurately understand

the mechanism of hepatotoxicity induced by AFM1 and OTA, it would be better to consider combining the obtained metabolomics results with other omics results in the future.

4. Materials and Methods

4.1. Chemicals and Reagents

AFM1 and OTA were purchased from Pribolab (Singapore). Alanine aminotransferase (ALT), aspartate aminotransferase (AST), total bilirubin (TBIL), and glutamyltransferase (GCT) assay kit were purchased from Beijing-XinChuangYuan (Beijing, China). Formic acid and acetonitrile (purity > 98% by HPLC) were obtained from Merck (Darmstadt, Germany). The enhanced cell counting kit-8 (CCK-8) was obtained from Beyotime Biotechnology (Shanghai, China). Dulbecco's modified eagle's medium (DMEM), fetal bovine serum (FBS), antibiotics (10,000 units/mL penicillin and 10,000 µg/mL streptomycin), and non-essential amino acids solution (NEAA) were purchased from GIBCO (Grand Island, NY, USA).

4.2. Animals and Treatment

Sixty CD-1 mice (20 ± 2 g, male) were obtained from Beijing Vital River Laboratory Animal Technology Co., Ltd. (Beijing, China). These mice were fed in the SPF barrier system under the condition of 22 ± 1 °C and $50 \pm 5\%$ humidity in China Agricultural University. The animal experiments conducted in the present study were approved by the Ethics Committee of Institute of Animal Sciences, Chinese Academy of Agriculture Sciences (Beijing, China), with the permission code of "IAS2019-3 (Date: 18/3/2019)".

The mice were randomly separated into five treatments: control treatment (free-feeding), DMSO vehicle treatment (1.0% DMSO), AFM1 treatment (3.5 mg/kg b.w.), OTA treatment (3.5 mg/kg b.w.), and the combination of AFM1 and OTA treatment (3.5 mg/kg b.w. AFM1 + 3.5 mg/kg b.w. OTA). The stock solution of AFM1 and OTA were 700 mg/L and 900 mg/L, respectively, which were dissolved in 0.5% DMSO/ddH₂O. The dose of AFM1 and OTA used in the present study was demonstrated in our previous study [57]. The mice in DMSO and toxins' treatment were gavaged once a day (0.2 mL/mice), lasting for 35 days. After treatment, the mice were euthanized by CO₂. The liver tissue was collected, weighed, and frozen in liquid nitrogen for subsequent histological assessment and metabolomic analysis.

4.3. Determination of Liver Index and Serum Biochemical Indicators

The relative liver weight (liver index) was calculated as the formula: $\text{liver index\%} = \text{liver weight} / \text{final weight of the mice} \times 100$. The final weight of the mice was measured before the blood collection. The collection of serum samples was the same as previously reported [62]. The serum biochemical indicators related to liver function, including ALT, AST, TBIL, and GCT were measured following the introductions of enzyme-linked immunosorbent assay (ELISA) kits.

4.4. Histopathological Assessment of Liver

Liver tissues were fixed with 4% paraformaldehyde solution for 24 h, a part of liver samples was dehydrated in alcohol, embedded in paraffin wax with a thickness of 4 mm section, followed by sliced at 5 µm, stained with HE using light microscopy (Nikon Corporation, Tokyo, Japan). Another part of liver tissue was dehydrated in sucrose solution, embedded in optimal cutting temperature compound, followed by being sliced at 8–10 µm and stained with ORO by light microscopy (Nikon Corporation, Tokyo, Japan) to identify the lipid droplets in the tissue. Lipid droplets are orange-red to bright red, and the nucleus are blue. The area of lipid droplets was quantified by Image-Pro Plus 6.0 software, and the percentage of lipid droplets area was calculated as the formula: $\% \text{ lipid droplets area} = \text{area of lipid droplets} / \text{area of liver tissue} \times 100$.

4.5. Cell Culture and Treatment

Human hepatocellular carcinoma cells (HepG2 cells) were obtained from ATCC (Manassas, VA, USA). The cells were cultured in an incubator at 37 °C with 5% CO₂ with the medium of DMEM supplemented with 10% FBS, 1% antibiotics, and 1% NEAA. HepG2 cells were seeded in a 96-well plate at the density of 1×10^5 cells/well and incubated for 24 h. The cells were then treated with AFM1 (0.2, 0.5, 0.8, 1.0, 1.5, 2.0, 3.0, 4.0 and 5.0 µg/mL) and OTA (0.01, 0.02, 0.03, 0.04, 0.05, 0.06, 0.07, 0.08, 0.10, 0.20 and 0.30 µg/mL). The cell viability was measured by CCK-8 assay following the manufacturer's instructions. Viability (%) = Mean OD in toxin group / Mean OD in control group \times 100.

In the present study, HepG2 cells exposed to 1.0 µg/mL AFM1 and 0.05 µg/mL OTA were used in the subsequent metabolomics analysis. The stock solution of AFM1 and OTA for *in vitro* experiment were 200 µg/mL and 1000 µg/mL, respectively. Therefore, the concentration of DMSO in the AFM1 and OTA used in the study was 0.5% and 0.005%, respectively.

4.6. Metabolomics Analysis

The sample (mice liver, mice serum and HepG2 cells) preparation was conducted. The liver sample in pre-cooled methanol was centrifuged at $1200 \times g$ for 10 s at 4 °C to obtain the liver supernatant. Centrifuging the serum sample in methanol: water solution at $1200 \times g$ for 15 min at 4 °C, and then the supernatant of serum was collected. HepG2 cells were incubated at 4 °C with shaking at $150 \times g$ for 30 min, and then centrifuged at $10,000 \times g$ for 10 min to collect the supernatant. The collected supernatant of liver, serum, and cell samples were dried in a vacuum evaporator and then detected via LC-MS. Each liver and serum group were composed of ten samples, and each cell group was composed of six samples.

The conditions of UPLC-MS metabolomics assay were reported as our previous study [56]. The instrument parameters were referenced to the previous method [63] and conducted by LipidALL Technologies Co., Ltd. (Changzhou, China). The raw data files were extracted using extracted by MarkerView 1.3 (AB Sciex, Concord, ON, Canada). The metabolites were identified by BMDB (<http://www.rumendb.ca/cgi-bin/browse.cgi> (accessed on 29 November 2021)), HMDB (<http://www.hmdb.ca/> (accessed on 29 November 2021)), METLIN (https://metlin.scripps.edu/landing_page.php?pgcontent=mainPage (accessed on 29 November 2021)) databases. The principal component analysis (PCA) was conducted on all data which is used to analyze the clustering of the analysis data of each group and remove abnormal samples. Afterwards, a supervised data analysis was carried out on the differences between the divisions, mainly using orthogonal projections to latent structures discriminant analysis (OPLS-DA). PCA and OPLS-DA analysis were conducted on Metaboanalyst 3.0 (Montréal, QC, Canada). CytoScape 3.4.0. (Boston, MA, USA) was used to draw the network mapping. The differentially expressed metabolites were screened with a criterion of variable importance in projection (VIP) >1 and $p < 0.05$.

4.7. Statistical Analysis

GraphPad Prism 8.0 (La Jolla, CA, USA) was applied in the present study to perform the data analysis. Significant differences among treatments were assessed using one-way ANOVA test followed by Tukey's multiple comparisons, which represents as $p < 0.05$.

Supplementary Materials: The following are available online at <https://www.mdpi.com/article/10.3390/toxins14020141/s1>, Figure S1: Metabolite integrated metabolic pathway analysis in liver of mice treated with individual and combined AFM1 and OTA. (A) Control vs AFM1, (B) Control vs OTA, (C) Control vs AFM1+OTA and (D) the number of changed metabolites in different mycotoxins treatment. Red represents the upregulated metabolites, and the green represents the downregulated metabolites with criterion of FC > 1.50 , and $p < 0.05$; Figure S2: Metabolite integrated metabolic pathway analysis in serum of mice treated with individual and combined AFM1 and OTA. (A) Control vs AFM1, (B) Control vs OTA, (C) Control vs AFM1+OTA and (D) the number of changed

metabolites in different mycotoxins treatment. Red represents the upregulated metabolites, and the green represents the downregulated metabolites with criterion of $FC > 1.50$, and $p < 0.05$; Figure S3: The concentration of significant changed LysoPCs in liver; Figure S4: The concentration of significant changed LysoPCs in serum; Figure S5: Cytotoxic effects induced by AFM1 and OTA on HepG2 cells; Figure S6: Heat map representation of metabolites in the HepG2 cell under different conditions of mycotoxins treatment. Red and blue represent higher and lower level of the respective metabolites. C represents control group, A represents individual AFM1 group, O represents OTA group and H represents AFM1+OTA group; Figure S7: The concentration of significant changed LysoPCs in HepG2 cells.

Author Contributions: Conceptualization, Y.-N.G.; methodology, C.-Q.W.; data curation, C.-Q.W.; writing—original draft preparation, Y.-N.G.; writing—review and editing, N.Z.; supervision, J.-Q.W. All authors have read and agreed to the published version of the manuscript.

Funding: This research was funded by the National Natural Science Foundation of China (31972190), China Agriculture Research System of MOF and MARA, the Agricultural Science and Technology Innovation Program (ASTIP-IAS12), and the Scientific Research Project for Major Achievements of Agricultural Science and Technology Innovation Program (CAAS-ZDXT2019004).

Institutional Review Board Statement: The study was conducted according to the Chinese guidelines for animal care, conforming to internationally accepted principles for the care and utilization of experimental animals. Animal experiments were approved by the Ethics Committee of the Chinese Academy of Agricultural Sciences (Beijing, China), with the permission code of “IAS2019-3 (Date: 18 March 2019)”.

Informed Consent Statement: Not applicable.

Data Availability Statement: Data are available upon request; please contact the contributing authors.

Acknowledgments: We are grateful to Guangzhou Genedenovo Biotechnology Co., Ltd. for assisting in sequencing and bioinformatics analysis.

Conflicts of Interest: The authors declare no conflict of interest.

References

1. Eskola, M.; Kos, G.; Elliott, C.T.; Hajslova, J.; Mayar, S.; Krska, R. Worldwide contamination of food-crops with mycotoxins: Validity of the widely cited ‘FAO estimate’ of 25. *Crit. Rev. Food Sci. Nutr.* **2020**, *60*, 2773–2789. [[CrossRef](#)] [[PubMed](#)]
2. Fromme, H.; Gareis, M.; Volkel, W.; Gottschalk, C. Overall internal exposure to mycotoxins and their occurrence in occupational and residential settings—An overview. *Int. J. Hyg. Environ. Health* **2016**, *219*, 143–165. [[CrossRef](#)] [[PubMed](#)]
3. IARC (International Agency for Research on Cancer). IARC (International Agency for Research on Cancer). IARC Monographs on the Evaluation of Carcinogenic Risks to Humans. 82. Aflatoxins: B1, B2, G1, G2, M1. In *Some Traditional Herbal Medicines, Some Mycotoxins, Naphthalene, and Styrene*; World Health Organization: Lyon, France, 2002; Volume 82, pp. 171–175.
4. Iqbal, S.Z.; Jinap, S.; Pirouz, A.A.; Ahmad Faizal, A.R. Aflatoxin M1 in milk and dairy products, occurrence and recent challenges: A review. *Trends Food Sci. Technol.* **2015**, *46*, 110–119. [[CrossRef](#)]
5. Li, S.; Min, L.; Wang, P.; Zhang, Y.; Zheng, N.; Wang, J. Aflatoxin M1 contamination in raw milk from major milk-producing areas of China during four seasons of 2016. *Food Control* **2017**, *82*, 121–125. [[CrossRef](#)]
6. Li, S.; Min, L.; Wang, P.; Zhang, Y.; Zheng, N.; Wang, J. Occurrence of aflatoxin M1 in pasteurized and UHT milks in China in 2014–2015. *Food Control* **2017**, *78*, 94–99. [[CrossRef](#)]
7. Zheng, N.; Sun, P.; Wang, J.Q.; Zhen, Y.P.; Han, R.W.; Xu, X.M. Occurrence of aflatoxin M1 in UHT milk and pasteurized milk in China market. *Food Control* **2013**, *29*, 198–201. [[CrossRef](#)]
8. Lee, H.J.; Ryu, D. Worldwide Occurrence of Mycotoxins in Cereals and Cereal-Derived Food Products: Public Health Perspectives of Their Co-occurrence. *J. Agric. Food Chem.* **2017**, *65*, 7034–7051. [[CrossRef](#)]
9. Mousavi Khaneghah, A.; Fakhri, Y.; Raeisi, S.; Armoon, B.; Sant’Ana, A.S. Prevalence and concentration of ochratoxin A, zearalenone, deoxynivalenol and total aflatoxin in cereal-based products: A systematic review and meta-analysis. *Food Chem. Toxicol.* **2018**, *118*, 830–848. [[CrossRef](#)]
10. Marin, D.E.; Braicu, C.; Dumitrescu, G.; Pistol, G.C.; Cojocneanu, R.; Neagoe, I.B.; Taranu, I. MicroRNA profiling in kidney in pigs fed ochratoxin A contaminated diet. *Ecotoxicol. Environ. Saf.* **2019**, *184*, 109637. [[CrossRef](#)]
11. Ostry, V.; Malir, F.; Toman, J.; Grosse, Y. Mycotoxins as human carcinogens—the IARC Monographs classification. *Mycotoxin Res.* **2017**, *33*, 65–73. [[CrossRef](#)]
12. Brera, C.; Debegnach, F.; De Santis, B.; Pannunzi, E.; Berdini, C.; Prantera, E.; Gregori, E.; Miraglia, M. Simultaneous determination of aflatoxins and ochratoxin A in baby foods and paprika by HPLC with fluorescence detection: A single-laboratory validation study. *Talanta* **2011**, *83*, 1442–1446. [[CrossRef](#)] [[PubMed](#)]

13. Elaridi, J.; Dimassi, H.; Hassan, H. Aflatoxin M1 and ochratoxin A in baby formulae marketed in Lebanon: Occurrence and safety evaluation. *Food Control* **2019**, *106*, 106680. [[CrossRef](#)]
14. Turkoglu, C.; Keyvan, E. Determination of Aflatoxin M1 and Ochratoxin A in Raw, Pasteurized and UHT Milk in Turkey. *Acta Sci. Vet.* **2019**, *47*, 1626. [[CrossRef](#)]
15. Saad-Hussein, A.; Elserougy, S.; Beshir, S.; Ibrahim, M.I.M.; Awad, A.H.A.; Abdel-Wahhab, M.A. Work-related airborne fungi and the biological levels of mycotoxin in Textile workers. *J. Appl. Sci. Res.* **2012**, *8*, 719–726.
16. Mekuria, A.N.; Routledge, M.N.; Gong, Y.Y.; Sisay, M. Aflatoxins as a risk factor for liver cirrhosis: A systematic review and meta-analysis. *BMC Pharm. Toxicol.* **2020**, *21*, 39. [[CrossRef](#)]
17. Deng, Z.J.; Zhao, J.F.; Huang, F.; Sun, G.L.; Gao, W.; Lu, L.; Xiao, Q. Protective Effect of Procyanidin B2 on Acute Liver Injury Induced by Aflatoxin B1 in Rats. *Biomed. Environ. Sci.* **2020**, *33*, 238–247. [[CrossRef](#)]
18. Li, X.; Lv, Z.; Chen, J.; Nepovimova, E.; Long, M.; Wu, W.; Kuca, K. *Bacillus amyloliquefaciens* B10 can alleviate liver apoptosis and oxidative stress induced by aflatoxin B1. *Food Chem. Toxicol.* **2021**, *151*, 112124. [[CrossRef](#)]
19. Xu, Q.; Shi, W.; Lv, P.; Meng, W.; Mao, G.; Gong, C.; Chen, Y.; Wei, Y.; He, X.; Zhao, J.; et al. Critical role of caveolin-1 in aflatoxin B1-induced hepatotoxicity via the regulation of oxidation and autophagy. *Cell Death Dis.* **2020**, *11*, 6. [[CrossRef](#)]
20. Marin, D.E.; Pistol, G.C.; Gras, M.; Palade, M.; Taranu, I. A comparison between the effects of ochratoxin A and aristolochic acid on the inflammation and oxidative stress in the liver and kidney of weanling piglets. *Naunyn Schmiedeberg's Arch. Pharm.* **2018**, *391*, 1147–1156. [[CrossRef](#)]
21. Wang, W.; Zhai, S.; Xia, Y.; Wang, H.; Ruan, D.; Zhou, T.; Zhu, Y.; Zhang, H.; Zhang, M.; Ye, H.; et al. Ochratoxin A induces liver inflammation: Involvement of intestinal microbiota. *Microbiome* **2019**, *7*, 151. [[CrossRef](#)]
22. Zhai, S.S.; Ruan, D.; Zhu, Y.W.; Li, M.C.; Ye, H.; Wang, W.C.; Yang, L. Protective effect of curcumin on ochratoxin A-induced liver oxidative injury in duck is mediated by modulating lipid metabolism and the intestinal microbiota. *Poult. Sci.* **2020**, *99*, 1124–1134. [[CrossRef](#)]
23. Zhang, H.; Yan, A.; Liu, X.; Ma, Y.; Zhao, F.; Wang, M.; Looor, J.J.; Wang, H. Melatonin ameliorates ochratoxin A induced liver inflammation, oxidative stress and mitophagy in mice involving in intestinal microbiota and restoring the intestinal barrier function. *J. Hazard. Mater.* **2021**, *407*, 124489. [[CrossRef](#)] [[PubMed](#)]
24. Johnson, C.H.; Ivanisevic, J.; Siuzdak, G. Metabolomics: Beyond biomarkers and towards mechanisms. *Nat. Rev. Mol. Cell Biol.* **2016**, *17*, 451–459. [[CrossRef](#)]
25. Xie, G.; Sun, J.; Zhong, G.; Shi, L.; Zhang, D. Biodistribution and toxicity of intravenously administered silica nanoparticles in mice. *Arch. Toxicol.* **2010**, *84*, 183–190. [[CrossRef](#)] [[PubMed](#)]
26. Li, S.; Liu, R.; Wei, G.; Guo, G.; Yu, H.; Zhang, Y.; Ishfaq, M.; Fazilani, S.A.; Zhang, X. Curcumin protects against Aflatoxin B1-induced liver injury in broilers via the modulation of long non-coding RNA expression. *Ecotoxicol. Environ. Saf.* **2021**, *208*, 111725. [[CrossRef](#)] [[PubMed](#)]
27. Eraslan, G.; Essiz, D.; Akdogan, M.; Karaoz, E.; Oncü, M.; Özyildiz, Z. Efficacy of dietary sodium bentonite against subchronic exposure to dietary aflatoxin in broilers. *Bull. Vet. Inst. Pulawy* **2006**, *50*, 107–112.
28. Lu, X.; Hu, B.; Shao, L.; Tian, Y.; Jin, T.; Jin, Y.; Ji, S.; Fan, X. Integrated analysis of transcriptomics and metabolomics profiles in aflatoxin B1-induced hepatotoxicity in rat. *Food Chem. Toxicol.* **2013**, *55*, 444–455. [[CrossRef](#)]
29. Moore, D.L.; Henke, S.E.; Fedynich, A.M.; Laurenz, J.C.; Morgan, R. Acute effects of aflatoxin on northern bobwhites (*Colinus virginianus*). *J. Wildl. Dis.* **2013**, *49*, 568–578. [[CrossRef](#)]
30. Wang, H.; Li, W.; Muhammad, I.; Sun, X.; Cui, X.; Cheng, P.; Qayum, A.; Zhang, X. Biochemical basis for the age-related sensitivity of broilers to aflatoxin B1. *Toxicol. Mech. Methods* **2018**, *28*, 361–368. [[CrossRef](#)]
31. Gayathri, L.; Dhivya, R.; Dhanasekaran, D.; Periasamy, V.S.; Alshatwi, A.A.; Akbarsha, M.A. Hepatotoxic effect of ochratoxin A and citrinin, alone and in combination, and protective effect of vitamin E: *in vitro* study in HepG2 cell. *Food Chem. Toxicol.* **2015**, *83*, 151–163. [[CrossRef](#)]
32. Hou, L.; Liu, S.; Zhao, C.; Fan, L.; Hu, H.; Yin, S. The combination of T-2 toxin and acrylamide synergistically induces hepatotoxicity and nephrotoxicity via the activation of oxidative stress and the mitochondrial pathway. *Toxicol.* **2021**, *189*, 65–72. [[CrossRef](#)]
33. Pyo, M.C.; Shin, H.S.; Jeon, G.Y.; Lee, K.W. Synergistic interaction of ochratoxin A and acrylamide toxins in human kidney and liver cells. *Biol. Pharm. Bull.* **2020**, *43*, 1346–1355. [[CrossRef](#)] [[PubMed](#)]
34. Sun, L.H.; Lei, M.Y.; Zhang, N.Y.; Zhao, L.; Krumm, C.S.; Qi, D.S. Hepatotoxic effects of mycotoxin combinations in mice. *Food Chem. Toxicol.* **2014**, *74*, 289–293. [[CrossRef](#)] [[PubMed](#)]
35. Ji, J.; Zhu, P.; Cui, F.; Pi, F.; Zhang, Y.; Li, Y.; Wang, J.; Sun, X. The Antagonistic Effect of Mycotoxins Deoxynivalenol and Zearalenone on Metabolic Profiling in Serum and Liver of Mice. *Toxins* **2017**, *9*, 28. [[CrossRef](#)] [[PubMed](#)]
36. Cui, J.; Yin, S.; Zhao, C.; Fan, L.; Hu, H. Combining Patulin with Cadmium Induces Enhanced Hepatotoxicity and Nephrotoxicity *in vitro* and *in vivo*. *Toxins* **2021**, *13*, 221. [[CrossRef](#)]
37. Dong, Y.; Qiu, P.; Zhao, L.; Zhang, P.; Huang, X.; Li, C.; Chai, K.; Shou, D. Metabolomics study of the hepatoprotective effect of *Phellinus igniarius* in chronic ethanol-induced liver injury mice using UPLC-Q/TOF-MS combined with ingenuity pathway analysis. *Phytomedicine* **2020**, *74*, 152697. [[CrossRef](#)]
38. Sun, M.; Zhang, J.; Liang, S.; Du, Z.; Liu, J.; Sun, Z.; Duan, J. Metabolomic characteristics of hepatotoxicity in rats induced by silica nanoparticles. *Ecotoxicol. Environ. Saf.* **2021**, *208*, 111496. [[CrossRef](#)]

39. Xu, L.; Tang, X.; Hao, F.; Gao, Y. Hepatotoxicity and nephrotoxicity assessment on ethanol extract of Fructus Psoraleae in Sprague Dawley rats using a UPLC-Q-TOF-MS analysis of serum metabolomics. *Biomed. Chromatogr.* **2021**, *35*, e5064. [[CrossRef](#)]
40. Sun, Y.; Wang, X.; Zhou, Y.; Zhang, J.; Cui, W.; Wang, E.; Du, J.; Wei, B.; Xu, X. Protective effect of metformin on BPA-induced liver toxicity in rats through upregulation of cystathionine beta synthase and cystathionine gamma lyase expression. *Sci. Total Environ.* **2021**, *750*, 141685. [[CrossRef](#)]
41. Zhang, Y.; Wang, Q.; Wang, Z.X.; Bi, Y.N.; Yuan, X.M.; Song, L.; Jiang, M.M.; Sun, L.K.; Zhou, K. A Study of NMR-Based Hepatic and Serum Metabolomics in a Liver Injury Sprague-Dawley Rat Model Induced by Psoralen. *Chem. Res. Toxicol.* **2018**, *31*, 852–860. [[CrossRef](#)]
42. Ji, J.; Zhu, P.; Blazenovic, I.; Cui, F.; Gholami, M.; Sun, J.; Habimana, J.; Zhang, Y.; Sun, X. Explaining combinatorial effects of mycotoxins Deoxynivalenol and Zearalenone in mice with urinary metabolomic profiling. *Sci. Rep.* **2018**, *8*, 3762. [[CrossRef](#)] [[PubMed](#)]
43. Tan, Y.; Yin, P.; Tang, L.; Xing, W.; Huang, Q.; Cao, D.; Zhao, X.; Wang, W.; Lu, X.; Xu, Z.; et al. Metabolomics study of stepwise hepatocarcinogenesis from the model rats to patients: Potential biomarkers effective for small hepatocellular carcinoma diagnosis. *Mol. Cell. Proteom.* **2012**, *11*, M111010694. [[CrossRef](#)] [[PubMed](#)]
44. Oh, H.A.; Lee, H.; Park, S.Y.; Lim, Y.; Kwon, O.; Kim, J.Y.; Kim, D.; Jung, B.H. Analysis of plasma metabolic profiling and evaluation of the effect of the intake of Angelica keiskei using metabolomics and lipidomics. *J. Ethnopharmacol.* **2019**, *243*, 112058. [[CrossRef](#)] [[PubMed](#)]
45. Liu, Y.; Wang, R.; Zheng, K.; Xin, Y.; Jia, S.; Zhao, X. Metabonomics analysis of liver in rats administered with chronic low-dose acrylamide. *Xenobiotica* **2020**, *50*, 894–905. [[CrossRef](#)] [[PubMed](#)]
46. Yoo, H.J.; Jung, K.J.; Kim, M.; Kim, M.; Kang, M.; Jee, S.H.; Choi, Y.; Lee, J.H. Liver Cirrhosis Patients Who Had Normal Liver Function Before Liver Cirrhosis Development Have the Altered Metabolic Profiles Before the Disease Occurrence Compared to Healthy Controls. *Front. Physiol.* **2019**, *10*, 1421. [[CrossRef](#)] [[PubMed](#)]
47. Olsvik, P.A.; Skjaerven, K.H.; Softeland, L. Metabolic signatures of bisphenol A and genistein in Atlantic salmon liver cells. *Chemosphere* **2017**, *189*, 730–743. [[CrossRef](#)]
48. Cuykx, M.; Rodrigues, R.M.; Laukens, K.; Vanhaecke, T.; Covaci, A. *in vitro* assessment of hepatotoxicity by metabolomics: A review. *Arch. Toxicol.* **2018**, *92*, 3007–3029. [[CrossRef](#)]
49. Yu, J.; Zhang, H.; Li, Y.; Sun, S.; Gao, J.; Zhong, Y.; Sun, D.; Zhang, G. Metabolomics revealed the toxicity of cationic liposomes in HepG2 cells using UHPLC-Q-TOF/MS and multivariate data analysis. *Biomed. Chromatogr.* **2017**, *31*, e4036. [[CrossRef](#)] [[PubMed](#)]
50. Park, S.; Kim, J.A.; Choi, S.; Suh, S.H. Superoxide is a potential culprit of caspase-3 dependent endothelial cell death induced by lysophosphatidylcholine. *J. Physiol. Pharm.* **2010**, *61*, 375–381.
51. Tian, C.; Li, S.; He, L.; Han, X.; Tang, F.; Huang, R.; Lin, Z.; Deng, S.; Xu, J.; Huang, H.; et al. Transient receptor potential ankyrin 1 contributes to the lysophosphatidylcholine-induced oxidative stress and cytotoxicity in OLN-93 oligodendrocyte. *Cell Stress Chaperones* **2020**, *25*, 955–968. [[CrossRef](#)]
52. Zhao, Y.Y.; Lei, P.; Chen, D.Q.; Feng, Y.L.; Bai, X. Renal metabolic profiling of early renal injury and renoprotective effects of Poria cocos epidermis using UPLC Q-TOF/HSMS/MSE. *J. Pharm. Biomed. Anal.* **2013**, *81*, 202–209. [[CrossRef](#)] [[PubMed](#)]
53. Shi, J.; Zhou, J.; Ma, H.; Guo, H.; Ni, Z.; Duan, J.; Tao, W.; Qian, D. An *in vitro* metabolomics approach to identify hepatotoxicity biomarkers in human L02 liver cells treated with pekinenal, a natural compound. *Anal. Bioanal. Chem.* **2016**, *408*, 1413–1424. [[CrossRef](#)]
54. Montesano, A.; Senesi, P.; Vacante, F.; Mollica, G.; Benedini, S.; Mariotti, M.; Luzi, L.; Terruzzi, I. L-Carnitine counteracts *in vitro* fructose-induced hepatic steatosis through targeting oxidative stress markers. *J. Endocrinol. Investig.* **2020**, *43*, 493–503. [[CrossRef](#)] [[PubMed](#)]
55. Moosavi, M.; Rezaei, M.; Kalantari, H.; Behfar, A.; Varnaseri, G. L-carnitine protects rat hepatocytes from oxidative stress induced by T-2 toxin. *Drug Chem. Toxicol.* **2016**, *39*, 445–450. [[CrossRef](#)] [[PubMed](#)]
56. Gao, Y.; Wang, J.; Li, S.; Zhang, Y.; Zheng, N. Aflatoxin M1 cytotoxicity against human intestinal Caco-2 cells is enhanced in the presence of other mycotoxins. *Food Chem. Toxicol.* **2016**, *96*, 79–89. [[CrossRef](#)]
57. Wang, Z.; Gao, Y.; Huang, X.; Huang, S.; Yang, X.; Wang, J.; Zheng, N. Metabolomics analysis underlay mechanisms in the renal impairment of mice caused by combination of aflatoxin M1 and ochratoxin A. *Toxicology* **2021**, *458*, 152835. [[CrossRef](#)]
58. Gao, Y.; Li, S.; Bao, X.; Luo, C.; Yang, H.; Wang, J.; Zhao, S.; Zheng, N. Transcriptional and proteomic analysis revealed a synergistic effect of aflatoxin M1 and ochratoxin A mycotoxins on the intestinal epithelial integrity of differentiated human Caco-2 cells. *J. Proteome Res.* **2018**, *17*, 3128–3142. [[CrossRef](#)]
59. Gao, Y.; Li, S.; Wang, J.; Luo, C.; Zhao, S.; Zheng, N. Modulation of intestinal epithelial permeability in differentiated Caco-2 cells exposed to aflatoxin M1 and ochratoxin A individually or collectively. *Toxins* **2018**, *10*, 13. [[CrossRef](#)]
60. Gao, Y.; Ye, Q.; Bao, X.; Huang, X.; Wang, J.; Zheng, N. Transcriptomic and proteomic profiling reveals the intestinal immunotoxicity induced by aflatoxin M1 and ochratoxin A. *Toxicon* **2020**, *180*, 49–61. [[CrossRef](#)]
61. Huang, X.; Gao, Y.; Li, S.; Wu, C.; Wang, J.; Zheng, N. Modulation of mucin (MUC2, MUC5AC and MUC5B) mRNA expression and protein production and secretion in Caco-2/HT29-MTX co-cultures following exposure to individual and combined aflatoxin M1 and ochratoxin A. *Toxins* **2019**, *11*, 132. [[CrossRef](#)]

-
62. Gao, Y.; Bao, X.; Meng, L.; Liu, H.; Wang, J.; Zheng, N. Aflatoxin B1 and Aflatoxin M1 Induce Compromised Intestinal Integrity through Clathrin-Mediated Endocytosis. *Toxins* **2021**, *13*, 184. [[CrossRef](#)] [[PubMed](#)]
 63. Song, J.W.; Lam, S.M.; Fan, X.; Cao, W.J.; Wang, S.Y.; Tian, H.; Chua, G.H.; Zhang, C.; Meng, F.P.; Xu, Z.; et al. Omics-Driven Systems Interrogation of Metabolic Dysregulation in COVID-19 Pathogenesis. *Cell Metab.* **2020**, *32*, 188–202.e185. [[CrossRef](#)] [[PubMed](#)]